A Parabolized Navier-Stokes Prediction of Hypersonic Window Cooling

Gregory J. Banken* and Donald W. Roberts†
Amtec Engineering, Inc., Bellevue, Washington
and
J. Eric Holcomb‡ and Stanley F. Birch§
Boeing Aerospace Company, Seattle, Washington

An analysis tool has been developed for calculating the three-dimensional flowfield associated with slot cooling at hypersonic speeds. The work involves modifications to an existing PNS code to accommodate the more complex geometry encountered in slot-cooling applications and to extend the range of application of the code to hypersonic speeds. The major modification of the code required for the hypersonic calculations was the incorporation of a real gas model. It is demonstrated that this can be accomplished for a cost penalty, over the equivalent ideal gas calculation, of only 5 to 10%. The resulting code was used to conduct a parametric study of slot-cooling efficiency, including an angle-of-attack calculation. The influence of Mach number on the turbulent mixing rate of the slot flow is also discussed.

Nomenclature

a	= speed of sound
C	= constant
C_p	= specific heat (const p)
h	= enthalpy; heat-transfer coefficient
h_{SLOT}	= height of slot
K,k	= thermal conductivity; turbulence kinetic energy
M_o	= molecular weight
p,P	= pressure
Pr	= Prandtl number
R	= universal gas constant
Re	= Reynolds number
T	= temperature
T_{aw}	= adiabatic wall temperature
T_c	= coolant total temperature
T_H	= temperature of hot gas in surface boundary layer prior to start of window cooling
V	= flow velocity
V_c	= coolant slot flow exit velocity
z	= axial station on conical body
z_{SLOT}	= axial station of coolant slot exit
Z	= compressibility factor
α	= angle of attack
θ	= half-angle of cone
ρ	= fluid density
ρ_c	= density of coolant flow at slot exit
μ,μ_t,μ_a	= viscosity (laminar, turbulent, artificial)
∞	= freestream conditions
ϵ	= turbulence energy-dissipation rate
(ξ,η,σ)	= general coordinate system

Introduction

In recent years an increased interest in new hypersonic vehicle concepts has resulted in a growth in hypersonic research. These new vehicles range in complexity from ground-launched hypersonic missiles to the transatmospheric vehicle (TAV) that will take off from the earth, go into orbit, perform a mission, and then land back on earth. The design of these vehicles involves a number of fluid dynamic phenomena that are unique to the hypersonic flow regime. Of these, a dominant feature is the aerodynamic heating that results in high heat-transfer rates to the surfaces. Various methods have been developed to reduce the high heat-transfer rates. These include heat shields made of ablating or subliming materials and various types of transpiration cooling. For applications that require windows, however, these procedures may not be applicable. For these applications, the use of slot cooling, achieved by injecting a jet of cold gas from a tangential slot and blowing it over the window, is often the preferred method of cooling.

The growing cost of wind-tunnel testing, particularly for the hypersonic regime, and the difficulty of accurately simulating the full-scale flow in ground-based experimental facilities, makes an experimental-based design of a slot-cooling system for a hypersonic vehicle very difficult. Fortunately, recent advances in algorithm development, combined with advances in computer hardware design, have resulted in major advances in computational fluid dynamics (CFD) that are now starting to revolutionize our approach to hypersonic aerodynamics. Much work remains to be done, but available methods are already sufficiently advanced to be of direct use in the design process.

This paper discusses the development of a numerical method that is used to model a hypersonic missile flowfield that includes an embedded wall jet. The flow-analysis code solves the parabolized Navier-Stokes (PNS) equations. A real gas model and special boundary conditions to simulate a slot for the wall jet have been incorporated into the code. The PNS code has been used to perform parametric studies to optimize the cooling jet. A 3-D angle-of-attack case has also been run at a freestream Mach number of 15 with a wall jet on the windward side of the missile.

Analysis

Numerical Model

Since the flowfields around hypersonic vehicles are predominately supersonic, the steady Navier-Stokes equations have a parabolic character when applied to such flows. The flow properties at downstream locations are physically determined by only the upstream flow conditions. This allows the use of efficient numerical techniques based on a single pass,

Presented as Paper 85-1591 at the AIAA 18th Fluid Dynamics and Plasmadynamics and Lasers Conference, Cincinnati, OH, July 16-18, 1985; received Aug. 5, 1985; revision submitted Nov. 25, 1985.

*Engineer.
†Vice President.
‡Engineer. Member AIAA.
§Senior Specialist Engineer. Member AIAA.

streamwise marching procedure for advancing the solution of the governing equations. For viscous flows, a thin subsonic layer, where the Navier-Stokes equations are formally elliptic in the streamwise direction, must exist on the surface. By parabolizing the equations, a marching procedure can still be used in the subsonic layers. This approximation is generally accurate and stable as long as the subsonic layers are thin.

The flow-analysis code used in the present investigation is an extension of the method developed by Roberts and Forester[1] for modeling supersonic forebody flowfields. The parabolized Navier-Stokes (PNS) equations are transformed from Cartesian to a general curvilinear (ξ,η,σ) coordinate system. A simplification of the transformed flow equations is incorporated by requiring that the computational mesh planes be perpendicular to the z-coordinate, which is nominally the predominant flow direction. The resulting transport equations are given by the following:

Continuity:

$$(y_\eta \rho u)_\xi - (y_\xi \rho u)_\eta + (x_\xi \rho v)_\eta - (x_\eta \rho v)_\xi + (D\rho w)_\xi + (E\rho w)_\eta + (J\rho w/z_\sigma)_\sigma = 0 \tag{1a}$$

Momentum:

$$Fu_\xi + Gu_\eta + (J\rho w/z_\sigma)u_\sigma + y_\eta P_\xi - y_\xi P_\eta = L[u] \tag{1b}$$

$$Fv_\xi + Gv_\eta + (J\rho w/z_\sigma)v_\sigma + x_\xi P_\eta - x_\eta P_\xi = L[v] \tag{1c}$$

$$Fw_\xi + Gw_\eta + (J\rho w/z_\sigma)w_\sigma + DP_\xi + EP_\eta + (J/z_\sigma)P_\sigma = L[w] \tag{1d}$$

Energy:

$$FH_\xi + GH_\eta + (J\rho w/z_\sigma)H_\sigma = L[\mathrm{H}] + (1-Pr)L[h]/Pr \tag{1e}$$

where

$$L[\phi] = y_\eta\left(\mu\frac{y_\eta\phi_\xi - y_\xi\phi_\eta}{J}\right)_\xi - y_\xi\left(\mu\frac{y_\eta\phi_\xi - y_\xi\phi_\eta}{J}\right)_\eta + x_\xi\left(\mu\frac{x_\xi\phi_\eta - x_\eta\phi_\xi}{J}\right)_\eta - x_\eta\left(\mu\frac{x_\xi\phi_\eta - x_\eta\phi_\xi}{J}\right)_\xi + D\left(\mu\frac{D\phi_\xi + E\phi_\eta}{J}\right)_\xi + E\left(\mu\frac{D\phi_\xi + E\phi_\eta}{J}\right)_\eta$$

$$D = (x_\eta y_\sigma - 1x_\sigma y_\eta)/z_\sigma \qquad E = (y_\xi x_\sigma - x_\xi y_\sigma)/z_\sigma$$

$$F = y_\eta \rho u - x_\eta \rho v + D\rho w \qquad G = -y_\xi \rho u + x_\xi \rho v + E\rho w$$

$$J = x_\xi y_\eta - y_\xi x_\eta$$

Pressure is related to density and enthalpy by a state relation. For laminar flows, the viscosity, μ, is related to the fluid properties by either Sutherland's formula or real gas relationships. The transport equations are hyperbolic-parabolic in the sigma coordinate direction, since the streamwise diffusion terms have been neglected. The equations remain elliptic in the x-y plane. Implied in the parabolic approximation is the design of the numerical model to eliminate the possibility of the upstream propagation of pressure waves. The use of a single-pass marching procedure removes this possibility. Hence, all of the σ-derivatives are discretized using upwind differences. The other derivatives are modeled using central differences.

For turbulent flows, the Reynolds' stresses, which appear in the Reynolds-averaged Navier-Stokes equations, are modeled by adding the turbulence viscosity, μ_t, to molecular viscosity, μ, where

$$\mu_t = C_\mu \rho k^2/\epsilon \tag{2}$$

The turbulence kinetic energy, k, and its dissipation rate, ϵ, are calculated using two additional equations.[2]

$$Fk_\xi + Gk_\eta + (J\rho w/z_\sigma)k_\sigma = L[k]/C_k + JQ - J\rho\epsilon \tag{3a}$$

$$F\epsilon_\xi + G\epsilon_\eta + (J\rho w/z_\sigma) = L[\epsilon]/C_\epsilon + JC_1(\epsilon/k)Q - JC_2\rho\epsilon^2/k \tag{3b}$$

where

$$Q = \mu_t \tau_{ij}(\partial u_i/\partial x_j)$$

$$\tau_{ij} = (\partial u_i/\partial x_j + \partial u_j/\partial x_i)$$

The last two terms in Eqs. (3) represent the production and dissipation.

The method for calculating the implicit pressure field is unlike typical hyperbolic numerical formulations. The present approach preserves the lateral-plane ellipticity of the pressure field and alleviates the acoustical stiffness of the continuity equation in the subsonic layer. The continuity equation (1a) is formulated to be mass conservative for a computational cell where the metric coefficients are projections of the cell face areas. When mass is conserved for each cell, global mass conservation is achieved. The velocity and density fields available after the momentum and energy equations are solved will initially not satisfy continuity. By assuming that the local continuity error results from an incorrect pressure field, a method for adjusting the pressure field such that all the governing equations are simultaneously updated can be developed.

The effect of a local pressure perturbation, P', on the local crossflow velocity components, u and v, is determined from the discrete form of the momentum equations, assuming that the streamwise convection term is dominant.

$$u' = \tfrac{1}{2} z_\sigma (y_\eta - y_\xi)P'/(J\rho w)$$

$$v' = -\tfrac{1}{2} z_\sigma (x_\xi - x_\eta)P'/(J\rho w)$$

For an isentropic perturbation, the effect of P' on density is

$$\rho' = P'/a^2$$

By adding u', v' and ρ' to u, v, and ρ and substituting into the discrete form of the continuity equation, the following relation for P' is derived:

$$P' = \omega(\text{Continuity Error})/(A - B/a^2)$$

where A and B are collections of terms involving metrics, velocities, and densities, and ω is a relaxation factor. The local continuity error drives the local pressure field. An iterative procedure is used to update P, ρ, u, and v until the continuity error reaches a given tolerance on each cell. The enthalpy may also be included in the iterative update procedure. The resulting implicit pressure field is elliptic. The effects of the updated variables on the w-velocity component are felt as the solution is iterated at each computational plane.

The existence of departure solutions when using hyperbolic marching techniques in subsonic wall layers has led to several different sublayer approximations for handling the P_σ term in Eq. (1d). The current PNS code does not use a sublayer approximation in the momentum equations. However, during the pressure-continuity iteration procedure the density at subsonic points is held fixed until the iteration is terminated. Departure solutions have not been observed with the current method, even when several subsonic points exist in the boundary layer. However, no deliberate attempt has been made to force a departure solution.

The freestream flow conditions for velocity, density, and enthalpy are imposed as the boundary conditions on the outer mesh boundary which lies beyond the bow shock. The bow shock is captured as part of the solution; therefore, the outer mesh boundary is always positioned beyond the shock. The vehicle surface forms the inner boundary on which a no-slip boundary condition is enforced. The wall temperature can be specified or an adiabatic boundary condition can be used. For turbulent flows, the compressible form of the law-of-the-wall is used to generate the correct wall-shear stress and boundary conditions for the k and ϵ equations.

Since the differencing scheme is second-order accurate in the lateral plane, the resulting finite-difference equations inherently produce oscillations near regions where the mesh is insufficient to resolve sharp changes in the gradients of the flow variables. The bow shock is the most obvious candidate for generating this computational noise, but other regions of the flow domain such as the boundary layer can cause problems. The bow shock is particularly troublesome at hypersonic Mach numbers, since small oscillations can lead to negative temperatures that ultimately destroy the solution. To control the noise, numerical damping schemes have been employed. A pressure-activated artificial viscosity is calculated from

$$\mu_a C_a \frac{|\delta\delta P|}{P}$$

where $\delta\delta P$ is the local second difference of pressure. The local μ_a is added to the physical viscosity except next to the wall. Limiters are used to keep μ_a below the explicit stability limit. A mass-flux conservative artificial diffusion term has been added to the continuity equation, with μ_a as the diffusion coefficient. This damping scheme works well in the vicinity of the shock where pressure oscillations are prevalent. In the boundary layers, where the pressure is nearly constant, the effects of artificial viscosity are negligible. Typically, the diffusion coefficient is chosen such that the bow shock is captured within three or four mesh intervals. A fourth difference smoothing term has been added to each transport equation except continuity. This term tends to damp the spurious peaks and valleys that may occur. A filtering routine has also been incorporated into the code to locate short-wavelength noise in a particular flow variable and then eliminate the noise. This scheme is used only occasionally for the turbulence quantities.

The set of discretized nonlinear flow equations are solved using an iterative ADI marching scheme. Iteration between two computational planes is used to reduce the errors associated with the nonlinearities in the streamwise direction. The solution is initialized by inputting the initial mesh plane and flow conditions. A poor set of initial conditions can set up transients that can severely affect the solution. In this situation, substantial global damping is often required. The momentum and energy equations are solved using the ADI algorithm to obtain the velocity components and total enthalpy at the downstream plane. The pressure-continuity scheme is iterated until the continuity error reaches a specified tolerance or until a specified iteration limit is reached. Finally, the turbulence model equations are solved for k and ϵ, and μ_t is calculated. The flow equations are iterated at each plane until convergence or an iteration limit is achieved.

Equilibrium Air Properties

Hansen[3] points out that the ideal gas representation of air becomes invalid at static temperatures in excess of approximately 3600°R (2000 K). Beyond this point, the impact of the dissociation and ionization of the various constituents of air on the thermodynamic and transport properties must be taken into account. To this end, the PNS flow-analysis code offers the option between the ideal gas relationships and the real gas relationships developed by Tannehill and associates.[4,5] These relationships consist of simplified curve fits for the thermodynamic properties of equilibrium air, as taken from the NASA-RGAS routines. The range of validity for these curve fits is the same as the NASA-ARC RGAS program, namely, temperatures up to 25,000 K and densities from 10^{-7} to 10^{+3} amagats.

The specific curve fits used in this study were $h=h(p,\rho)$ and $T=T(p,\rho)$, as developed by Tannehill and Mugge.[5] However, the formulation of the state equation used in this PNS code required $\rho=\rho(p,h)$. Therefore, the first curve fit was used in a Newton-Raphson method to solve for density when given pressure and enthalpy. This modification in the application of the curve fit did not seriously impact the solution time, since the latest density for each mesh cell is used as the starting point for the next iterative search. As such, most cells required only one or two passes through the curve fit.

As a further enhancement on solution speed, the real gas effects for each mesh point were stored in an array and used for several iterations of the pressure-continuity scheme before another call was made to the curve fits. This was accomplished by using the equation of state:

$$\rho = PM_0/(ZRT)$$

Since ρ, p, and T are known following each call to the real gas routine, the ratio M_0/ZR can be computed, saved, and used on several subsequent pressure-continuity iterations assuming that, over the small variation in conditions typically seen between iterations, the curve fits are linear and, therefore, the ratio remains constant.

The result of the use of curve fits and storing the real gas effects was a calculation penalty, over the equivalent ideal gas calculations, of only 5 to 10%.

Coolant Slot Modeling

The modeling of a three-dimensional embedded coolant jet required the addition of program variables to describe the dimensions of the slot and variable boundary conditions. Figure 1 shows a perspective view of the 3-D geometry considered.

In practice the PNS solution is marched up to the exit plane of the coolant jet, and the program is stopped. At this point, the restart file, with the various flow properties at the mesh points, has the flow properties of the coolant slot appended to it by an external mesh and flow property generator. The solution control file is modified to reflect the location of the coolant jet and the desired boundary conditions as a function of body position.

Upon solution restart, the computational space would look like the example in Fig. 2. This particular example is set up to model one-half of an axisymmetric body. As seen from the

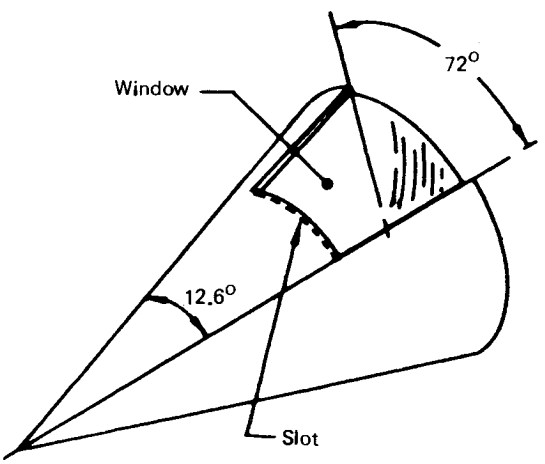

Fig. 1 View of model with window and slot.

figure, a portion of the mesh space is unused with this method. Instead of a true multizone solution approach, this method controls the starting point of the solution sweeps and the application of the appropriate boundary conditions in order to model the presence of an embedded coolant jet. Although the coolant slot boundaries are required to follow constant mesh lines, an irregular-shaped coolant slot can be modeled through changes to the computational mesh shape.

Cooling Effectiveness Study

Geometry and Flight Conditions Modeled

The first use of the coolant slot modeling capability was to perform a parametric study of cooling effectiveness as a function of freestream conditions, coolant mass flux, and slot height. The simplifying assumption of axisymmetric flow was made to increase the number of cases considered in the available time. With this assumption, the procedure for restarting the code at the slot exit is particularly simple, which allowed multiple computer runs to be made using the same initial solution.

Figure 3 shows the geometry and summarizes the flight conditions simulated. Only matched exit pressure conditions were considered. The calculations used a grid with 8-to-10 cells across the slot height, and approximately 35 total cells radially. Three points were used in the circumferential direction to model an axisymmetric body.

Another assumption in this study concerned the thermal boundary condition at the cone surface. Since the recovery temperature for equilibrium air flow at Mach 15 will approach 9000°R (5000 K), thermal protection is required over the entire vehicle, not just the window. Since the specific method of providing such protection is not the topic of this study, the study assumed that a constant wall temperature of 4000°R (2200 K) can be maintained up to the window station.

Finally, the flows under consideration were turbulent, except for a short region near the nose tip. Therefore, real gas routines were not used to calculate laminar viscosity or Prandtl number.

Computational Considerations

The sudden introduction of an embedded coolant slot flow on the external flow solution required that precautions be taken to ensure solution accuracy. Specifically, to minimize the nonphysical effects of artificial viscosity on the mixing of the coolant with the hot boundary-layer flow, the smoothing coefficients were set to zero in the momentum, energy, and turbulence model equations in the vicinity of the mixing layer. To reduce truncation errors, small marching steps were taken initially and then increased as the layer spread. To avoid the difficulties encountered in dealing with subsonic pockets in PNS formulations, all streamwise velocities were made supersonic when restarting the code.

Computation time for a series of runs, marching over the entire body for a single case, averaged 1 CPU minute or less on a Cray-1/S.

Parametric Study Results

The raw data calculated by the PNS code consists of the temperature, density, and pressure profiles, along with velocity vectors and turbulence quantities, at selected body stations. For example, Fig. 4 depicts the wall temperature rise as a function of cooling distance for three different coolant flow rates on a 12.6 deg cone at the nominal flight condition of Mach 15 and 100,000 ft (30.5 km) altitude. The gas temperature at the surface rises sharply after the mixing layer touches the surface, with the sharpest rise occurring for small flow rates.

Heat-transfer rates to the window surface, required for design purposes, were estimated by using the Reynolds

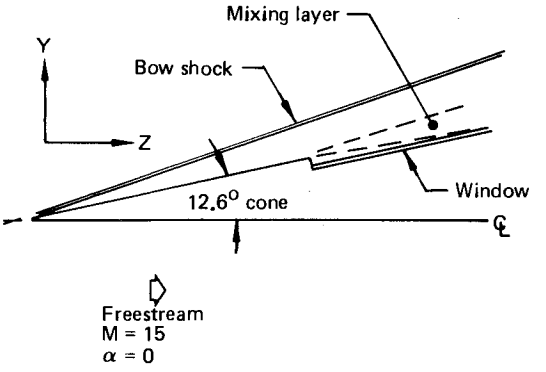

- Vehicle geometry
  - Cone half-angle = 12.6 deg
  - Slot geometry: Tangential flow injection
    - Step-down slot (axisymmetric)
    - Conformal window
  - Slot station (Z_{slot}) = 12.0 to 21.7 in.(30.5 to 55.1 cm)
  - Slot height (h_{slot}) = 0.10 to 0.25 in.(2.54 to 6.35 mm)
  - Window length = 6.0 to 12.0 in.(15.2 to 30.5 cm)
- Flight conditions
  - Mach = 7.0 to 15.0
  - Altitude = 70 to 100 kft (21.3 to 30.5 km)
  - Angle-of-attack = zero
- Coolant flow conditions
  - Static pressure ratio = 1.0
  - Velocity ratio = 0.10 to 0.33
  - Total temperature = 540°R (300°K)

Fig. 3 Geometry and flight conditions for cooling-effectiveness study.

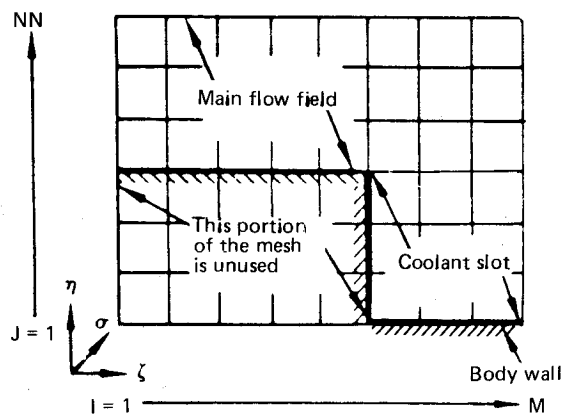

Fig. 2 Computational mesh for coolant slot modeling.

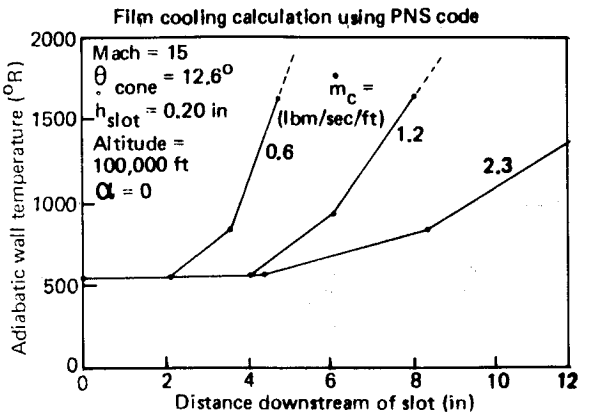

Fig. 4 Wall temperature rise vs distance from slot.

analogy between skin friction and heat transfer:

$$h = \mu_t C_P \frac{1}{V_e}\left(\frac{dV}{dy}\right)_w$$

where

μ_t = turbulent "eddy" viscosity
C_P = specific heat of air (const. P)
V_e = estimated velocity at edge of wall boundary layer
$(dV/dy)w$ = wall velocity gradient based on u at first mesh point away from wall.

Such a procedure should serve as a reliable guide to estimate instantaneous local heat-transfer rates, even though the calculation assumes steady flow and does not account for transient heating effects.

Figure 5 presents dimensional heat-transfer coefficients versus cooling distance for the nominal flight condition. It may seem unusual at first to observe that the coefficient increases with added coolant mass flow. This behavior, however, is consistent with the developing boundary layers in the three cases. By far the more important effect of the coolant is to reduce the gas-to-window-surface temperature differential (Fig. 4). As the boundary layer and mixing layer develop, the coefficient approaches the sharp cone value (dashed line on Fig. 5). Turbulent heat-transfer coefficients may be approximately scaled for other conditions using the Eckert formula as a guide:

$$h = 0.034(K^*/z)(Pr^*)^{1/3}(Re^*)^{4/5}$$

where $Re^* < 10^7$ and the asterisk denotes the Eckert reference temperature.[6]

For a more detailed parametric analysis, it is desirable to express the calculated results in terms of a functional relationship among dimensionless variables. For a fixed geometry, it is convenient to select the following variables:

Variable	Definition
Mach number	V_∞/a_∞
Coolant mass flux ratio	$\rho_c V_c/\rho_\infty V_\infty$
Cooling-distance ratio	$(Z-Z_{SLOT})/h_{SLOT}$
Cooling effectiveness	$(T_{aw}-T_H)/(T_c-T_H)$

Figures 6 and 7 illustrate cooling-effectiveness results expressed in this form, for Mach numbers of 7 and 15 on a 12.6 deg cone. Cooling length versus mass flux ratio may be approximately correlated via a 4/5-power law formula, similar to Eckert's formula for turbulent flow. The effect of flight conditions on thermal protection requirements is evident when comparing the two figures. Increasing Mach number, cone angle, and angle-of-attack all contribute to more severe heating. By normalizing the results with respect to flow properties inside the "inviscid" part of the shock layer, and forward of the window, it should be possible to develop a set of curves applicable over a range of flight conditions and geometries.

Figure 8 illustrates the linear dependence of cooling distance on slot height (hence coolant mass flow rate), attributed to the

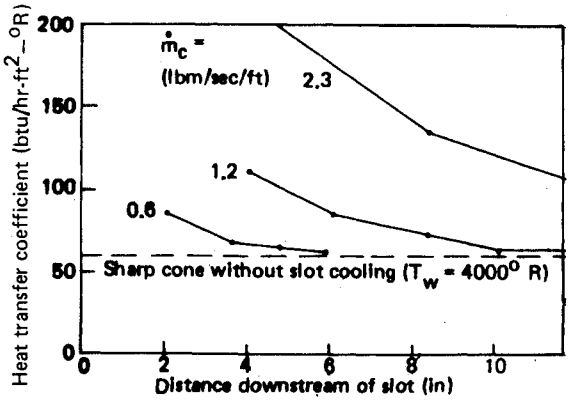

Note: Heat transfer coefficient increases with coolant mass flow due to delayed development of the slot flow boundary layer. The actual heat flux will decrease as more coolant is injected

Fig. 5 Heat-transfer coefficient versus distance from slot.

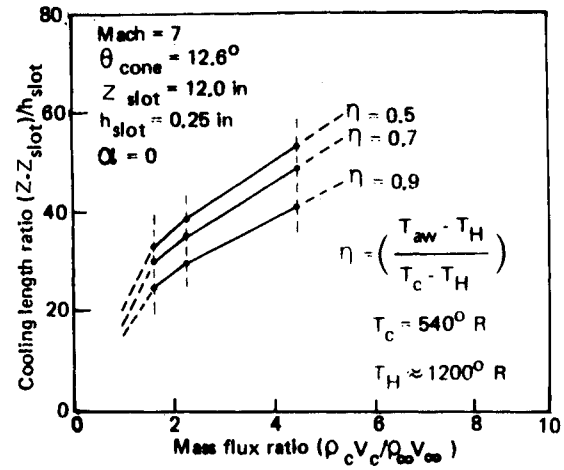

Fig. 6 Cooling effectiveness at Mach 7.

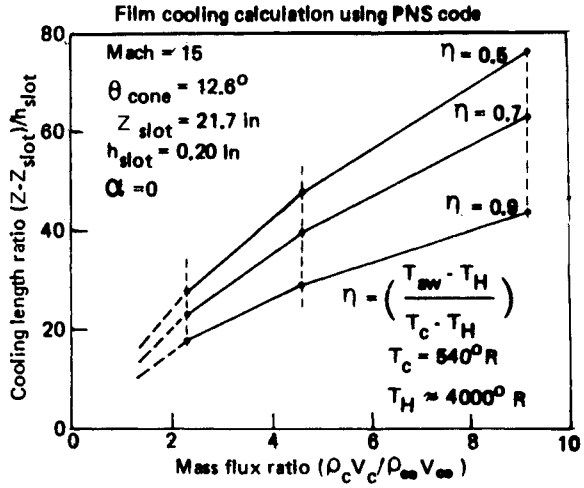

Fig. 7 Cooling effectiveness at Mach 15.

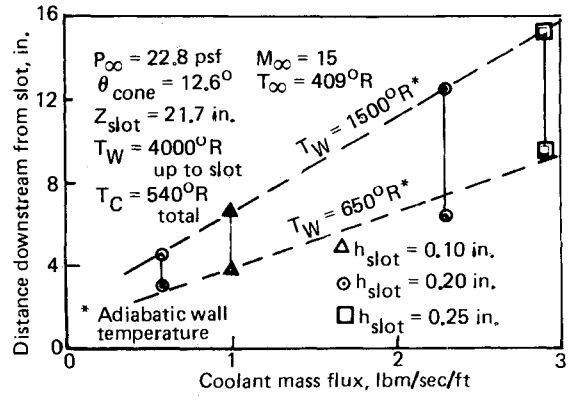

Fig. 8 Cooling length versus mass flux at Mach 15, altitude 100k ft.

nearly constant spreading rate of the mixing layer as the flow is convected downstream. Because the spreading rate in general can be a function of Mach number and velocity ratio (V_c/V_∞), these results may not hold for other conditions. (See section on "Mach Number Effects.")

Angle-of-Attack Calculation

The PNS flow-analysis code was also used to examine the effectiveness of slot cooling for a body at Mach 15, an altitude of 100,000 ft (30.5 km), and an angle of attack of 10 deg. The body shape was the same as that used in the parametric study (see Figs. 1 and 3). For this analysis, the coolant slot was oriented to the windward side of the body.

The computational mesh modeled one-half of the axisymmetric body and consisted of 35 circumferential grid points and 40 body radial grid points. Of this mesh, a 9×10 section modeled the 0.20-in.-high coolant slot flow. The grid spacing near the wall and throughout the coolant slot was 1.9% of the local shock standoff distance. Although additional mesh would have been appropriate to provide better flow resolution, this distribution was sufficient to resolve the main aspects of the flow, and to test the code.

A no-slip boundary condition was used over the entire exterior surface, including the coolant slot. A fixed wall temperature of 4000°R (2200 K) was specified on the exterior body surface, while an adiabatic wall condition was applied to the coolant slot surfaces. A law-of-the-wall was used to determine the shear forces along all wall surfaces.

Figure 9 illustrates a typical profile of the cross-flow velocities in the vicinity of the coolant slot, at a location approximately 16 slot heights downstream of the exit plane. The flow vectors within the coolant slot have not been adversely affected by the exterior flowfield. Similar results were seen at 50 slot heights downstream, thus eliminating concerns (at least for this condition) that the coolant flow would be "blown" out of the slot.

Figure 10 presents the pressure contours for the same location as Fig. 9. The figure depicts a well-developed flow about the body. The surface pressures are approximately 18% greater than those predicted by inviscid theory due to the compression wave generated by the initial mixing between the coolant flow and the external flow. This compression wave is more clearly seen in Fig. 11, which illustrates the pressure contours along the center axis of the window.

Figures 12 and 13 provide the associated flow temperature and density profiles along the center axis of the window. The calculation indicates that, for the analyzed coolant flux rate (i.e., $\rho_c V_c/\rho_\infty V_\infty$) of 24.3, adequate cooling was maintained for over 60 slot heights downstream.

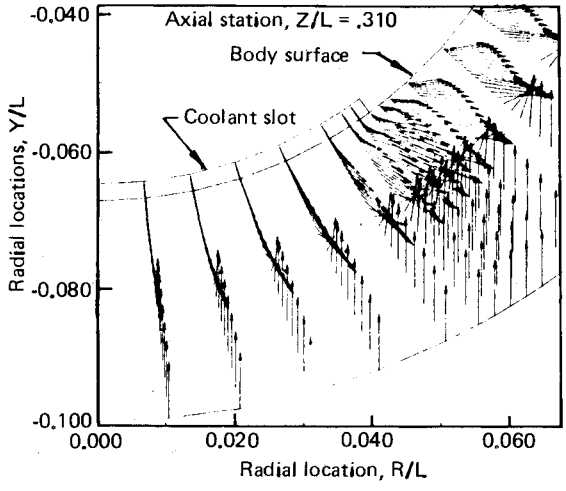

Fig. 9 Cross-flow velocity profile for $\alpha = 10$ deg.

The density profile in Fig. 13 illustrates the major problem introduced by film cooling for this application. The low-temperature flow required to provide effective cooling results in large and varying density gradients which, in turn, bend or refract the light in a varying manner. The bow shock will of course cause a similar effect. Together, the coolant flow and the bow shock will present a formidable problem to the success of any sensor which depends on light rays for detection. However, the use of flow-analysis tools such as the one described in this paper can provide a better understanding of

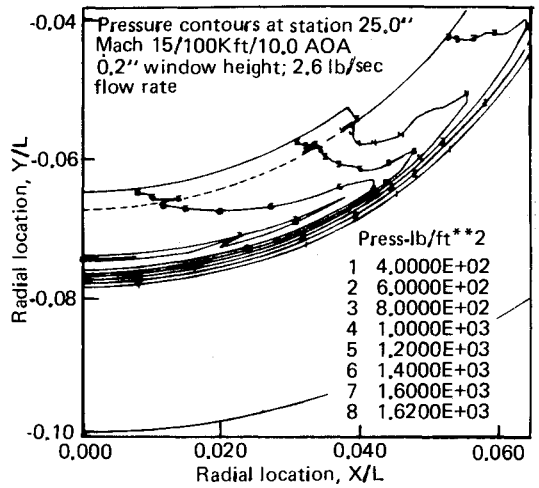

Fig. 10 Pressure contours for $\alpha = 10$ deg.

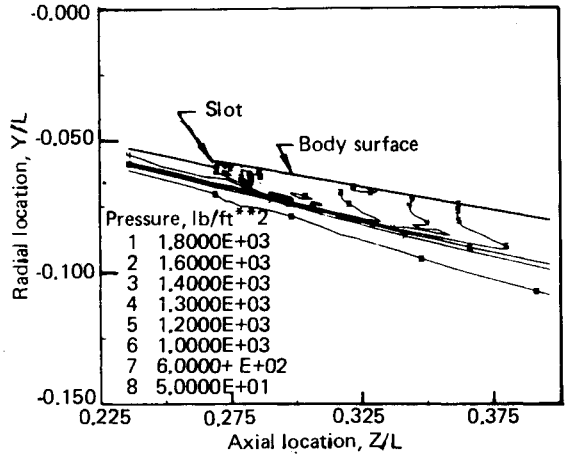

Fig. 11 Axial-pressure contours at window centerline for $\alpha = 10$ deg.

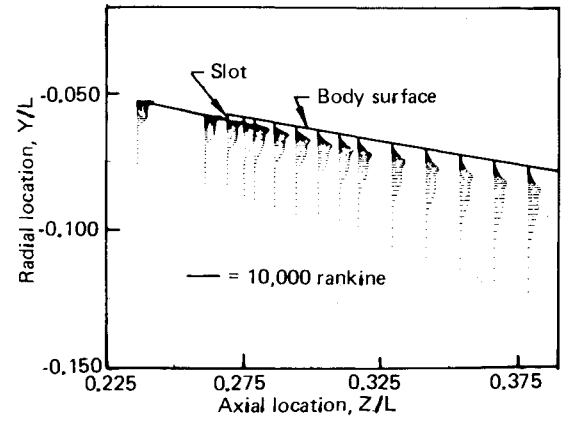

Fig. 12 Axial-temperature profile at window centerline for $\alpha = 10$ deg.

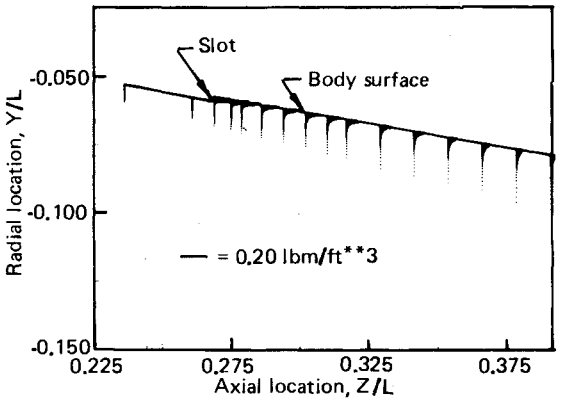

Fig. 13 Axial-density profile at window centerline for $\alpha = 10$ deg.

the density variations that will be encountered at different flight conditions.

Mach Number Effects

The effectiveness of the slot-cooling process is determined primarily by the mixing rate in the shear layer formed between the cool wall jet and the hot, high-Mach-number, external flow. It is well known[7] that the mixing rate in a planar mixing layer is a strong function of Mach number for Mach numbers greater than one. Initial conditions also have a strong influence on the mixing rate for a considerable distance downstream.[8] Unfortunately, detailed experimental data are at present limited to constant total temperature flows.

For the slot-cooling application considered here, and for most practical applications involving supersonic mixing layers, there is a strong total temperature gradient through the mixing layer. This introduces an uncertainty into any estimate of cooling effectiveness and highlights the need for detailed experimental data for supersonic mixing layers that are closer to those encountered in practical applications.

For the calculations presented here, the turbulent mixing was calculated using a standard two-equation k-ϵ turbulence model without any Mach number corrections. The resulting data were then scaled to approximately account for expected Mach number effects. The results are believed to be at least qualitatively correct, but additional work is obviously required.

Conclusions

An effective analysis tool for the study of hypersonic slot cooling flows has been developed and demonstrated. Much of the efficiency of the new analysis is due to the use of a relatively simple PNS marching algorithm, coupled with an efficient real gas routine. The resulting analysis was used to conduct a parametric study of slot cooling effectiveness. The major conclusions of this study were as follows:

1) The gas temperature at the window surface remains nearly constant until the mixing layer touches the surface, then rises sharply.

2) The length of window protected by the slot cooling flow is nearly directly proportional to the coolant mass flow rate (per unit width) and inversely proportional to the free stream mass flux (per unit area), for the range of conditions considered here.

3) The above conclusion appears to be nearly independent of slot height.

4) Large temperature and density gradients are present across the mixing layer at high Mach numbers.

5) Preliminary results indicate that slot cooling should be an effective means of thermal protection for angles-of-attack up to at least 10 deg.

6) A need has been identified for additional data to establish the turbulent mixing rate for high-Mach-number slot flows.

References

[1]Roberts, D. W. and Forester, C. K., "Three-Dimensional Viscous Supersonic Forebody Analysis," AFWAL-TR-81-3137, Air Force Wright Aeronautical Laboratories, Wright-Patterson AFB, Ohio, Dec. 1981.

[2]Launder, B. and Spalding, D. B., "The Numerical Computation of Turbulent Flows," *Computer Methods in Applied Mechanics and Engineering*, Vol. 3, 1974, pp. 259-289.

[3]Hansen, C. F., "Approximations for the Thermodynamic and Transport Properties of High-Temperature Air," NASA Tech. Rept. R-50, 1959.

[4]Tannehill, J. C. and Mohling, R. A., "Development of Equilibrium Air Computer Programs Suitable for Numerical Computation Using Time-Dependent or Shock-Capturing Methods," NASA CR-2134, Sept. 1972.

[5]Tannehill, J. C. and Mugge, P. H., "Improved Curve Fits for the Thermodynamic Properties of Equilibrium Air Suitable for Numerical Computation Using Time-Dependent or Shock-Capturing Methods," NASA CR-2470, Oct. 1974.

[6]Eckert, E. R. G., "Survey of Boundary Layer Heat Transfer at High Velocities and High Temperatures," WADC Tech. Rept. 59-624, April 1960.

[7]Birch, S. F. and Eggers, J. M., "A Critical Review of the Experimental Data for Developed Free Turbulent Shear Layers," NASA SP-321, Vol. 1: *Proceedings of the Conference on Free Turbulent Shear Flows*, NASA Langley Research Center, July 1972, pp. 11-40.

[8]Birch, S. F., "The Effect of Initial Conditions on High Reynolds Number Jets," AIAA Paper 83-1681, July 1983.